Variable-range hopping conductivity of La$_{1-x}$Sr$_x$Mn$_{1-y}$Fe$_y$O$_3$

Variable-range hopping conductivity of $La_{1-x}Sr_xMn_{1-y}Fe_yO_3$

V S Zakhvalinskii[1,2]**, R Laiho**[3]**, A V Lashkul**[1]**, K G Lisunov**[1,4]**,
E Lähderanta**[1,5]**, Yu S Nekrasova**[2]**, P A Petrenko**[4] **and
V N Stamov**[3,4]

[1] Department of Mathematics and Physics, Lappeenranta University of Technology,
PO Box 20, FIN-53851 Lappeenranta, Finland
[2] Department of Physics, Belgorod State University, RUS-308015 Belgorod, Russia
[3] Wihuri Physical Laboratory, University of Turku, FIN-20014 Turku, Finland
[4] Institute of Applied Physics, Academy of Sciences of Moldova, Academiei Street 5,
MD-2028 Kishinev, Moldova

E-mail: Erkki.Lahderanta@lut.fi

Abstract
The temperature dependence of the resistivity, ρ, of ceramic $La_{1-x}Sr_xMn_{1-y}Fe_yO_3$ (LSMFO)
samples with $x = 0.3$ and $y = 0.03, 0.15, 0.20$ and 0.25 (or simply #03, #15, #20 and #25,
respectively) is investigated between temperatures $T \sim 5$ and 310 K in magnetic fields B up to
8 T. Metallic conductivity in #03 is changed eventually to activated in #25. In #15 and #20 the
behavior of $\rho(T)$ is more complicated, comprising of two extremes, divided by an interval of
metallic behavior in #15, and two inflections of $\rho(T)$ in #20 within similar intervals ΔT below
~ 100 K. Mott variable-range hopping (VRH) conductivity is observed in #15 above the
ferromagnetic Curie temperature, T_C. In #20 the Mott VRH conductivity takes place in three
different temperature intervals at $T > T_C$, T close to T_C and $T < T_C$. In #25, the Mott VRH
conductivity is observed in two different intervals, above and below T_C, divided by an
intermediate interval of the Shklovskii–Efros VRH conduction regime. Analysis of the VRH
conductivity yielded the values of the localization radius, α, and the dependence of α and of the
density of the localized states, g, near the Fermi level, on B. Above T_C the localization radius in
all samples at $B = 0$ has similar values, $\alpha \approx 1.0–1.2$ Å, which is enhanced to $\alpha \approx 3.3$ Å (#20)
and 2.0 Å (#25) below T_C. The sensitivity of α and g to B depend on y and T. The complicated
behavior of the mechanisms of the hopping charge transfer, as well as of the microscopic
parameters α and g, is attributable to different electronic and magnetic phases of LSMFO
varying with temperature and Fe doping.

(Some figures in this article are in colour only in the electronic version)

1. Introduction

$La_{1-x}Sr_xMn_{1-y}Fe_yO_3$ (LSMFO) is a derivative of the
manganite perovskite compound $La_{1-x}Sr_xMnO_3$ (LSMO) [1],
obtained by substitution of Fe for Mn [2–6]. LSMFO belongs
to the family of colossal magnetoresistive (CMR) oxides [7],
thus making it a material of great interest. The basic properties
of the manganite perovskites and related CMR compounds,
such as existence of $Mn^{3+,4+}$ mixed valence states induced
by hole doping, competing ferromagnetic (FM) Mn^{3+}–Mn^{4+}
double-exchange (DE) and antiferromagnetic (AF) Mn^{3+}–
Mn^{3+} superexchange interactions, as well as local Jahn–
Teller distortions [8, 9] leading to formation of small lattice
polarons, have been found insufficient for interpretation of the
CMR effect [10, 11]. This has led to extensive experimental
and theoretical investigations, which have revealed such
interesting phenomena as phase separation and interplay
between the ordering of spin, charge and orbital degrees of
freedom [10, 11].

[5] Author to whom any correspondence should be addressed.

Usually, hole doping of the manganite perovskites is realized by the substitution of a divalent element Ca, Ba, or Sr for trivalent La, or by the formation of vacancies in the cation lattice of non-stoichiometric compounds [8, 9, 12, 13]. Weakly doped manganites exhibit mainly activated behavior of the resistivity, ρ, [8–10, 14]. Nearest-neighbor hopping (NNH) conductivity of small polarons has been observed in $La_{1-x}Ca_xMnO_3$ (LCMO) above room temperature up to 1200 K [14]. Below room temperature, microscopic disorder becomes important, leading to variable-range hopping (VRH) conductivity [9, 15]. VRH sets in when it is energetically favorable for a charge carrier to jump to sites beyond the nearest neighbors [16, 17].

Along with increased hole doping a temperature-induced metal–insulator transition (T-MIT) takes place in the manganite perovskites at a temperature T_{MI}, below which the conductivity is metallic [8, 9]. T_{MI} in manganites is usually close to the FM Curie temperature, T_C. In optimally doped manganites with the relative concentration of the holes $\sim$0.3, T_C can exceed the room temperature, as in LSMO with $x = 0.3$ [1, 8, 9]. On the other hand, T_C can be effectively decreased by doping with Fe, which has been found in LSMFO [4, 6] and in $La_{1-x}Ca_xMn_{1-y}Fe_yO_3$ (LCMFO) [18], favoring observation of the VRH conductivity. The point is that in manganites direct replacement of Mn^{3+} by Fe^{3+} [19] suppresses ferromagnetism, because Fe^{3+} does not support DE interactions in Fe^{3+}–Mn^{4+} pairs [20]. This leads to a decrease of T_C when y is increased. However, in LCMFO the decrease of T_C is much stronger than could be expected from only damping of the DE interactions [21], which can be explained by an increase of the microscopic disorder and the introduction of an additional fluctuating short-range potential, induced by doping with Fe [15].

Investigations of the VRH conductivity can yield useful information about the localization radius of charge carriers, α, and the density of the localized states (DOS), g, near the Fermi level, μ [17]. A reasonable order of the magnitude of $\alpha \sim 1$ Å, typical of small polarons, has been found in various CMR compounds [9, 22–24]. However, due to the simplified treatment of the DOS shape and the neglected temperature dependence of the resistivity prefactor, $\rho_0(T)$, it is difficult to estimate the accuracy of these results definitively. A more consistent approach to analysis of the VRH conductivity was done by taking into account the dependence of $\rho_0(T)$ and a complex structure of the DOS near μ, following from a scanning-tunneling spectroscopy study of $La_{1-x}Ca_xMnO_3$ (LCMO) [25]. This yielded more accurate values of α and features of the DOS spectrum such as the widths of the Coulomb gap and of the rigid (or hard) gap around μ in LCMFO [15], $La_{1-x}Ba_xMnO_3$ (LBMO) [26] and $LaMnO_{3+\gamma}$ (LMO) [27, 28]. On the other hand, the main goals in [15, 26–28] were to investigate the VRH conductivity only above T_C. Therefore, the investigations made in [15, 26–28] are still insufficient, because in weakly doped manganites the activated conductivity, attributable to the hopping charge transfer, persists for $T < T_C$ as well, although with more complicated behavior of $\rho(T)$ [1, 9, 15].

Based on the success in the investigations of the paramagnetic (PM) phase with $T > T_C$ mentioned above,

it is possible to expand the temperature region in order to characterize different phases of manganite perovskites by means of the hopping conductivity. Such a characterization is performed in this paper, together with the influence of Fe doping on the resistivity of LSMFO in general.

2. Experimental results

LSMFO samples with $x = 0.30$ and $y = 0$ to 0.25 were synthesized by a conventional solid state reaction method, similar to that used for preparation of LCMO [29], from La_2O_3, MnO_2, Fe_2O_3 and $SrCO_3$. The raw materials were pre-calcined to remove possible adsorbates, weighed in stoichiometric proportions, then mixed and subsequently heated in air at 1360 °C for 40 h with intermediate grindings. The mixtures were pressed into pellets and fired in air at 1500 °C for 22 h. According to x-ray diffraction data, the sample without Fe had an undistorted cubic structure (space group P_m3_m), whereas rhombohedral distortions (space group $R\bar{3}c$) were observed in the samples doped with Fe. The microprobe and scanning-tunneling microscopy analyses yielded grains sizes of a few micrometers for the LSMFO samples investigated with a homogeneous and stoichiometric distribution of the elements over the volume of the samples and within separate grains.

Investigations of $\rho(T, B)$ were made for $T \sim 5$–310 K using the conventional four-probe technique in the transverse magnetic field configuration ($\mathbf{B} \perp \mathbf{j}$) for $B = 0$ to 8 T. Magnetization $M(T)$ was measured with an RF-SQUID magnetometer after cooling the sample from room temperature down to 5 K in a zero dc field (M_{ZFC} or zero-field-cooled magnetization) or in fields of $B = 1$ and 100 mT (M_{FC} or field-cooled magnetization).

As can be seen in the top panel of figure 1, both $\chi_{ZFC}(T)$ and $\chi_{FC}(T)$ (where $\chi \equiv M/B$) in #15 and #20 exhibit a sharp FM transition in the field of $B = 1$ mT at the Curie temperature, T_C, defined by inflection points of the corresponding curves. The transition is accompanied by magnetic irreversibility or deviation of $\chi_{ZFC}(T)$ from $\chi_{FC}(T)$, implying frustration of the magnetic ground state of LSMFO. In #25 the FM transition is broadened appreciably, whereas the onset of the irreversibility is shifted from T_C towards higher temperatures. The magnetic irreversibility is damped strongly with increasing field (bottom panel of figure 1). On the other hand, one can see a considerable decrease of $\chi_{ZFC}(T)$ and $\chi_{FC}(T)$ with increasing y, whereas T_C decreases appreciably with y, as evident from the inset to the bottom panel of figure 1.

The zero-field resistivity of the LSMFO samples with $y = 0.03, 0.15, 0.20$ and 0.25, marked below as #03, #15, #20 and #25, respectively, are shown in the top panel of figure 2. The resistivity exhibits a strong dependence on y, similar to the behavior observed in [2]. In addition, the metallic character of $\rho(T)$ in #03 is changed eventually to a purely activated behavior of the resistivity in #25 within the whole interval of investigated temperatures. One should also note an inflection of $\rho(T)$ near T_C (marked with open triangles) in #15, weakening with increasing y and B, which is evident from the top and bottom panels of figure 2. In #15 and #20, the behavior of $\rho(T)$ is more complicated, comprising
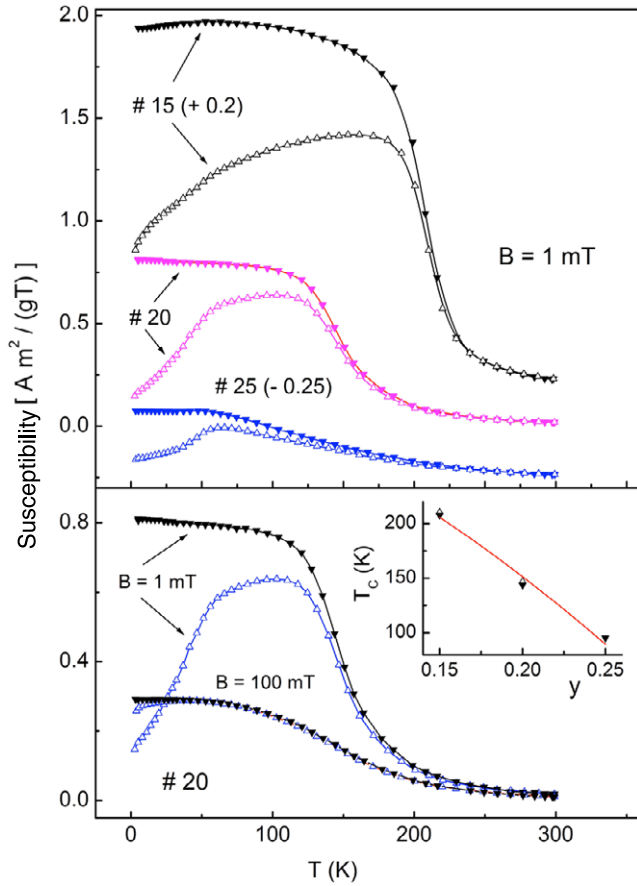
Figure 1. Top panel: temperature dependences of χ_{ZFC} ($\triangle$) and χ_{FC} ($\blacktriangledown$) in the investigated LSMFO samples at $B = 1$ mT. Some of the plots are shifted along the vertical axis by the values, given in parenthesis. Bottom panel: the plots of χ_{ZFC} versus T ($\triangle$) and χ_{FC} versus T ($\blacktriangledown$) in #20 at $B = 1$ and 100 mT. Inset: the dependence of T_C on y, obtained in the ZFC ($\triangle$) and FC ($\blacktriangledown$) regimes of cooling. The line is a fit with equation (6).
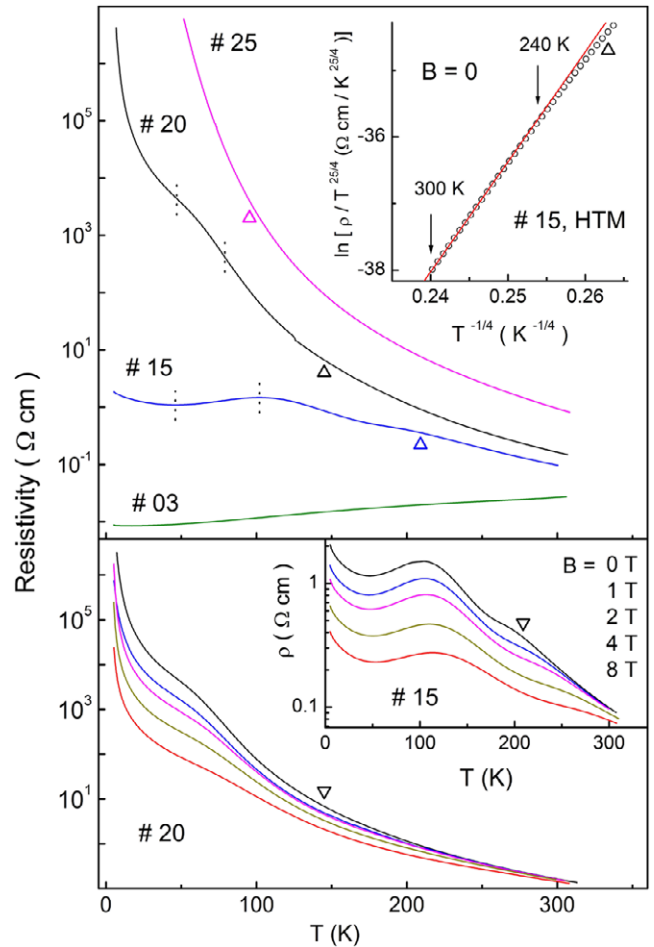
Figure 2. Top panel: temperature dependence of the resistivity in the investigated LSMFO samples at $B = 0$. The vertical dotted lines mark the extremes in #15 and inflections in #20 defining the interval ΔT (see the text). Inset: the plot of $\ln(\rho/T^{25/4})$ versus $T^{-1/4}$ at $B = 0$ for the interval HTM of #15. The line is a linear fit. The open triangles mark T_C. Bottom panel: the plots of ρ versus T at $B \geqslant 0$ in #15 and #20. T_C is given by the open triangle.

of two extremes divided by an interval of metallic behavior (downturn) in #15, and of two inflections of $\rho(T)$ in #20 within a similar temperature interval, ΔT, below $\sim$100 K. The extremes in #15 and inflections in #20, defining the interval ΔT, are marked in the top panel of figure 2 with the vertical dotted lines.

The large drop of the magnetoresistance (MR) of LSMFO shown in the bottom panel of figure 2, characteristic of the CMR effect in manganites [7–10], is enhanced considerably with increasing y from 0.15 to 0.20. Additionally, MR within the interval ΔT, defined above, is stronger than at temperatures around T_C, this feature being enhanced in #20 as well.

Hence, the behavior of the resistivity above is attributable to the hopping conduction in #20 and #25 both above and below T_C, and in #15 at $T > T_C$.

3. Theoretical background

The hopping conductivity is given by a universal expression,

$$\rho(T) = \rho_0(T) \exp[(T_0/T)^p], \qquad (1)$$

where the prefactor $\rho_0(T) = AT^m$, A is the prefactor constant and T_0 is the characteristic temperature [15, 17]. The exponents m and p are interrelated and depend on the mechanism of the hopping charge transfer. The NNH conductivity is given by $m = p = 1$. The VRH conductivity is described by the values of $p = 1/4$ (the Mott type) and $p = 1/2$ (the Shklovskii–Efros or SE type). The Mott VRH conductivity takes place when the Coulomb interactions between the carriers are unimportant [16]. Otherwise, such correlations lead to a soft Coulomb gap, Δ, in the DOS around μ and to the SE VRH conductivity [17]. In manganite perovskites the relation

$$m = 8 - p(7 + q) \qquad (2)$$

applies, where $q = 0$ for the absence and $q = 4$ for the presence of the contribution of a fluctuating short-range potential to the microscopic disorder, respectively [15]. The characteristic temperature in equation (1), $T_0 = T_{0M}$ and $T_0 = T_{SE}$ for the Mott and the SE VRH conductivity

Table 1. The values of A and T_0 in various temperature intervals of the VRH conductivity of investigated samples in zero field.

Sample	A (HTM) $(\Omega\,\mathrm{cm}\,\mathrm{K}^{-25/4})$	T_{0M} (HTM) (K)	A (ITM) $(\Omega\,\mathrm{cm}\,\mathrm{K}^{-25/4})$	T_{0M} (ITM) (K)	A (LTM) $(\Omega\,\mathrm{cm}\,\mathrm{K}^{-25/4})$	T_{0M} (LTM) (K)	A (SE) $(\Omega\,\mathrm{cm}\,\mathrm{K}^{-9/2})$	T_{SE} (K)
#15	1.92×10^{-34}	7.43×10^{8}	—	—	—	—	—	—
#20	2.79×10^{-35}	9.43×10^{8}	1.49×10^{-34}	8.16×10^{8}	1.29×10^{-19}	3.19×10^{7}	—	—
#25	6.49×10^{-39}	1.28×10^{9}	—	—	6.25×10^{-36}	2.0×10^{9}	5.59×10^{-19}	8.48×10^{4}

regimes, respectively, is given by the expressions

$$T_{0M} = \beta_M / [kg(\mu)\alpha^3] \qquad \text{and}$$
$$T_{SE} \approx [T_\delta^{1/2} + (T_\delta + T_{0SE})^{1/2}]^2, \qquad (3)$$

respectively [15, 17]. Here, $\beta_M = 21$ [17], $g(\mu)$ is the DOS at the Fermi level when the effects of the Coulomb gap are unimportant, $T_\delta = \delta_V^2/(4k^2 T_{VSE})$ and $T_{0SE} = \beta_{SE} e^2/(k\kappa\alpha)$ [17], where δ_V is the width of the rigid gap (existing inside Δ due to polaron effects in manganites [25, 27]) at the onset temperature, T_{VSE}, of the SE VRH conductivity, κ is the dielectric permittivity and $\beta_{SE} = 2.8$ [17]. The prefactor constant A is given for the manganite perovskites by the expression

$$A = C_0 \alpha^{11} T_0^{p(7+q)}, \qquad (4)$$

where $T_0 = T_{0M}$ at $p = 1/4$, $T_0 = T_{SE}$ at $p = 1/2$ and C_0 is a constant [15]. Finally, the value of the DOS outside the Coulomb gap, g_0, and Δ satisfy the expressions

$$g_0 = (3/\pi)(\kappa^3/e^6)(\Delta - \delta_V)^2 \qquad \text{and}$$
$$\Delta \approx k(T_{VSE} T_{SE})^{1/2}, \qquad (5)$$

respectively [15].

4. Analysis and discussion

4.1. Magnetic properties

Magnetic behavior of LSMFO shown in figure 1 is similar to that of LCMO [29], LCMFO [21], LBMO [30] and LMO [31], investigated previously. Here we concentrate only on the features, which will be useful for the subsequent analysis of the hopping conductivity of LSMFO. Expansion of the width of the FM transition in the bottom panel of figure 1 with increasing of B is attributable to the phase separation and increase of fraction of the second, hole-rich phase of the nanosize FM metallic particles (embedded into the PM or AF host lattice), which is sensitive to the applied magnetic field [11, 32]. The phase separation or inhomogeneous hole distribution leading to inclusions of the hole-rich FM metallic phase, is an intrinsic property of the CMR materials [11].

In low fields the effect of the phase separation on FM transition is expected to be relatively weak and T_C is given by the expression

$$kT_C \approx 0.05 W c (1 - c), \qquad (6)$$

where W is the width of the electron band and c is the concentration of the holes [33]. Taking into account that Fe^{3+} ions do not support the FM DE interactions [20] and

directly substitute Mn^{3+} in the lattice of manganites [19] (see section 1), as well as that doping with Fe causes only minor lattice distortions due to the close ionic radii of Fe^{3+} and Mn^{3+} [18], equation (6) can be utilized for the quantitative interpretation of $T_C(y)$ by putting $c \approx c_0 - y$ [21]. Here c_0 should be close to x, whereas the difference of $c_0 - x$ is connected to the cation vacancies (see section 1). Fit of the dependence of T_C on y, given by the solid line in the inset to the bottom panel of figure 1, yields the value of $W = 2.6 \pm 0.1$ eV, which is close to $W \approx 2.5$ eV in LSMO [33], and $c_0 = 0.31 \pm 0.01$.

4.2. Identification of the hopping conductivity mechanisms

The type of the hopping conductivity (NNH, Mott or SE VRH) can be determined by linearization of $\rho(T)$ in coordinates of $\ln(\rho/T^m)$ versus T^{-p}, taking into account the possible values of m and p, as well as equation (2) (see section 3). In particular, in #15 above T_C the best linearization of $\rho(T)$ is obtained for $p = 1/4$ and $m = 25/4$ (inset to the upper panel of figure 2). This correspond to the Mott VRH conductivity at the high-temperature interval HTM (marked by the vertical arrows) at $T > T_C$, where T_C is given by the open triangle, and to $q = 0$. The values of A and T_{0M}, obtained with a linear fit of the plot in the inset to the upper panel of figure 1, are collected in table 1.

As can be seen in the top panel of figure 3, the VRH conductivity with $p = 1/4$ and $m = 25/4$, corresponding to $q = 0$, is also observed in #20 in three different temperature intervals, exhibiting high-temperature Mott (HTM, $T > T_C$), intermediate-temperature Mott (ITM, T around T_C) and low-temperature Mott (LTM, $T < T_C$) behavior, characterized by different values of T_{0M} and A (table 1). In the top panel of figure 3, T_C is given by the open triangle and the limits of the corresponding intervals are marked by the vertical arrows.

Eventually, as shown in the bottom panel of figure 3, two intervals of the Mott VRH conductivity in #25 are observed at high (interval HTM between ≈ 220 and 170 K) and low (interval LTM with the onset near T_C, given by the open triangle) temperatures. The intervals of the Mott VRH conductivity in #25 are divided by that of the SE VRH conductivity (interval SE in the bottom panel of figure 3 between $T = T_{VSE} \approx 150$ K and T near T_C). The values of $m = 25/4$ in the intervals HTM and LTM, and $m = 9/2$ in the interval SE, correspond to $q = 0$ in #25, similar to #15 and #20. The prefactor constants and characteristic temperatures for the intervals HTM, SE and LTM of #25 are exhibited in table 1.

The above mechanisms of the hopping conductivity are found in zero magnetic field. It can be shown that the same behavior of the VRH conductivity takes place in #15 and
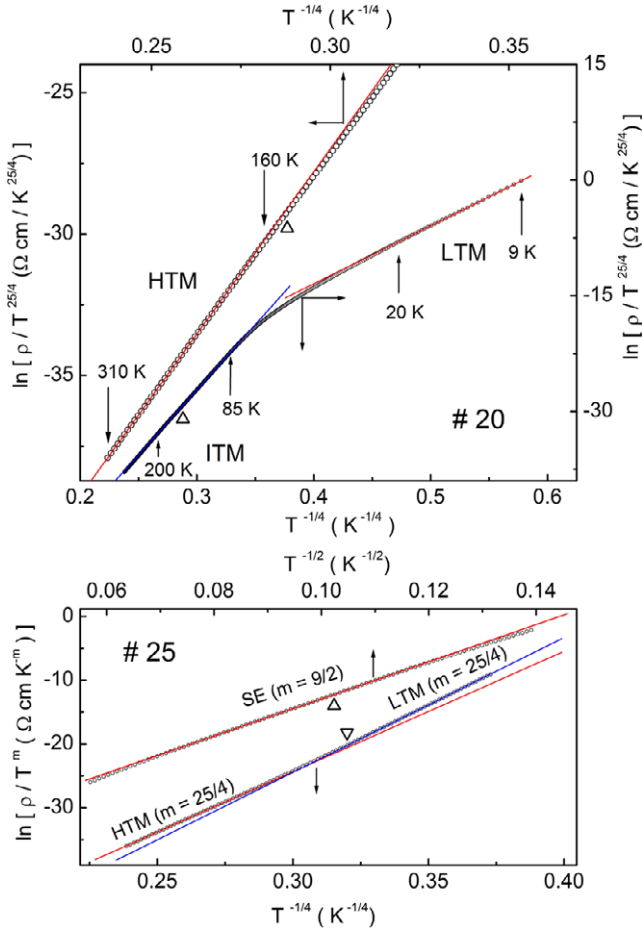
Figure 3. Top panel: the plots of $\ln(\rho/T^{25/4})$ versus $T^{-1/4}$ at $B = 0$ for the temperature intervals HTM, ITM and LTM of #20. The lines are linear fits. The open triangles mark $T_{\rm C}$. Bottom panel: the plots of $\ln(\rho/T^m)$ versus $T^{-1/2}$ and $T^{-1/4}$ for #25. The lines are linear fits. $T_{\rm C}$ is given by open triangles.
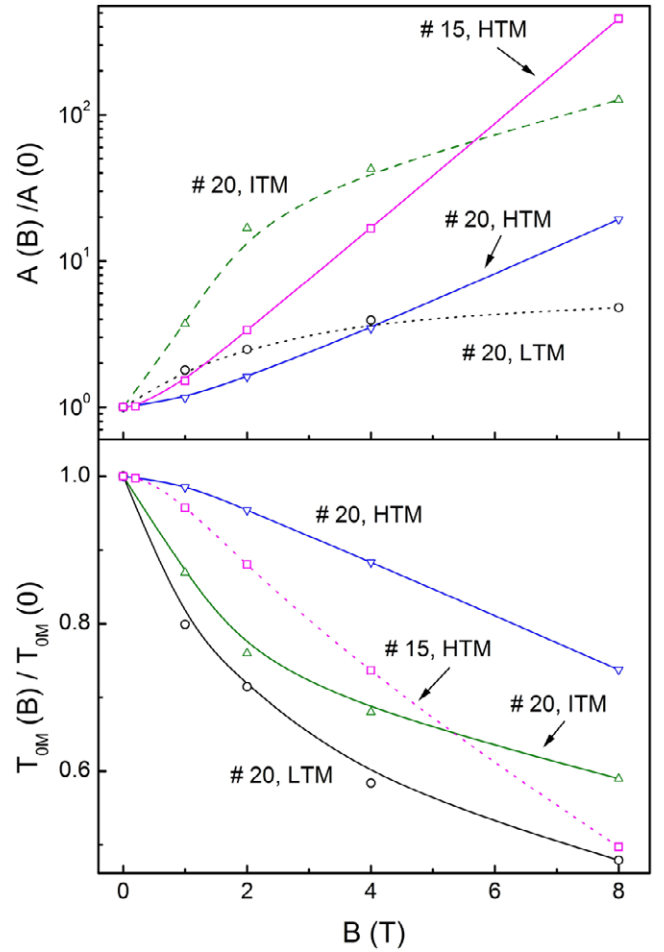
Figure 4. The dependences of $A(B)/A(0)$ (top panel) and $T_{\rm 0M}(B)/T_{\rm 0M}(0)$ (bottom panel) on the magnetic field, obtained in the temperature interval HTM of #15 and in different temperature intervals of #20. The lines are to guide the eye.

#20 in a field up to 8 T, but the width of the corresponding temperature intervals is decreased somewhat with increasing B. The dependences of the relative parameters $A(B)/A(0)$ and $T_{\rm 0M}(B)/T_{\rm 0M}(0)$ are displayed in figure 4.

4.3. Magnetic field dependence of the microscopic parameters

Due to the first of equations (3) and (4) the observed dependences of $A(B)/A(0)$ and $T_{\rm 0M}(B)/T_{\rm 0M}(0)$ in figure 4 are connected to the corresponding magnetic field dependences of the localization radius and DOS at the Fermi level. By solving this pair of equations over α and $g(\mu)$, one can find the variation of the relative parameters, $\alpha(B)/\alpha(0)$ and $g(B)/g(0)$ in a magnetic field, as shown in figure 5 as functions of B^2 along with the plots of $T_{\rm 0M}(B)/T_{\rm 0M}(0)$ versus B^2. Such a presentation of the data is used, because the relation

$$\alpha(B) = \alpha(0)(1 + b_a B^2) \tag{7}$$

has been predicted for the small-polaron radius of manganites in the PM phase, where b_a does not depend on B [33]. However, it can be seen in the middle panel of figure 5 that in

the temperature interval HTM of #15 and #20, defined above by the condition of $T > T_{\rm C}$ (attributable to the PM phase at $B = 0$), the quadratic behavior of $\alpha(B)$ can be addressed only to a relatively narrow region of $B \leqslant 2$ T. In addition, in the interval HTM below $B \sim 2$ T the variation of the DOS, g, and $T_{\rm 0M}$ with B approximately follows the behaviors

$$T_{\rm 0M}(B) \approx T_{\rm 0M}(0)(1 + b_T B^2) \qquad \text{and}$$
$$g(B) \approx g(0)(1 + b_g B^2), \tag{8}$$

respectively, where the coefficients b_T and b_g do not depend on B. The consistence of such behavior can be verified, provided that the conditions

$$b_g B^2 \ll 1 \qquad \text{and} \qquad 3b_a B^2 \ll 1 \tag{9}$$

are satisfied. Then, substituting equation (7) and the second of equations (8) into the first of equations (3), one can find in the first non-vanishing approximation over the magnetic field the relation
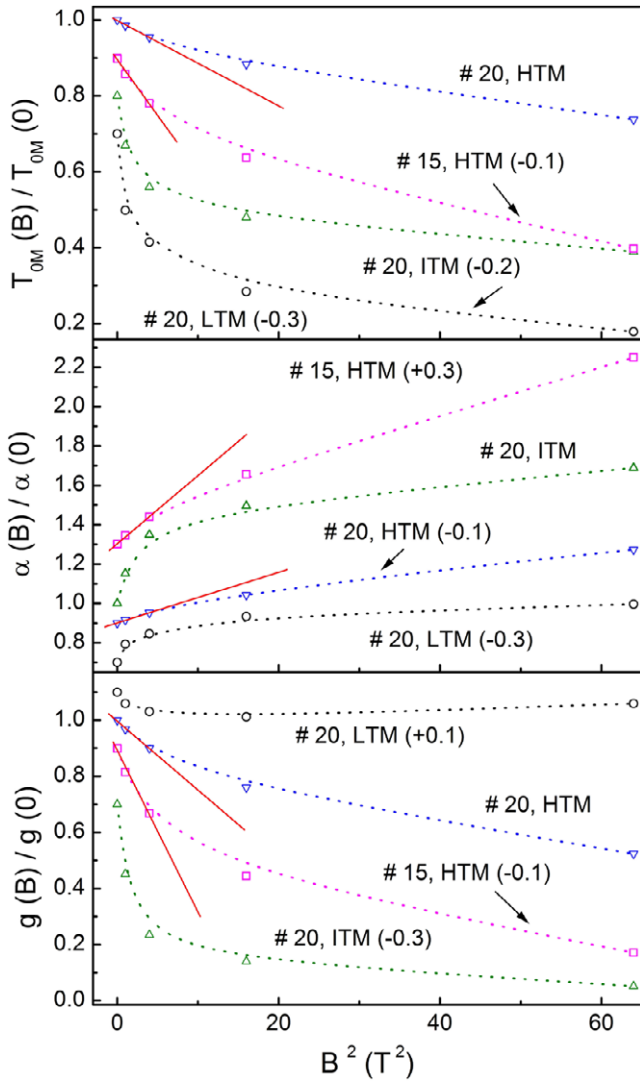
$$b_T \approx -(b_g + 3b_a). \tag{10}$$

Figure 5. The plots of $T_{0M}(B)/T_{0M}(0)$ versus B^2 (top panel), $\alpha(B)/\alpha(0)$ versus B^2 (middle panel) and $g(B)/g(0)$ versus B^2 (bottom panel) for the interval HTM of #15 and for different temperature intervals of #20. The dotted lines are to guide the eye and the solid lines are linear fits. For convenience some of the plots are shifted along the vertical axis by the values shown in parenthesis.

The linear fits of the plots in figure 5 up to $B = 2$ T, shown by the solid lines, yield for #20 the coefficients $b_T \approx -0.0112$, $b_a \approx 0.0129$ and $b_g \approx -0.0246$ (in T^{-2}), which gives for the right-hand side of equation (10) the value -0.0139 T^{-2}, agreeing reasonably with the value of the left-hand side of equation (10) or b_T. The corresponding parameters for #15, $b_T \approx -0.029$, $b_a \approx 0.035$ and $b_g \approx -0.058$ (in T^{-2}) give for the right-hand side of equation (10) the value -0.047 T^{-2}, also comparable with that of b_T. Although the difference between both sides of equation (10) for #15 is larger, this can be explained by the worsening of the conditions given by equation (9), where $3b_a B^2 \approx 0.42$ at $B = 2$ T is already comparable with unity. Taking this into account, one can infer that equation (10) is fulfilled satisfactorily for both samples, however, only for $B \leqslant 2$ T.

Table 2. The values of $g(\mu)$ and α in various temperature intervals of the VRH conductivity of the investigated samples at $B = 0$.

Sample	$g(\mu)$, (10^{20} eV^{-1} cm^{-3})	α (HTM) (Å)	α (ITM) (Å)	α (LTM) (Å)	α (SE) (Å)
#15	3.1	1.0	—	—	—
#20	2.1	1.1	1.1	3.3	—
#25	1.2	1.2	—	1.0	2.0

4.4. Determination of microscopic parameters at $B = 0$

The characteristic temperatures, collected in table 1, can be used to determine the zero-field values of α, provided that the corresponding values of DOS are known. The latter can be found with the expression [9, 22]

$$g(\mu) \approx N_s c(1 - c)/(2W), \qquad (11)$$

where $c \approx c_0 - y$, $c_0 \approx 0.31$, $W \approx 2.6$ eV (see section 4.1), $N_s \approx N_0(1 - y)$ and $N_0 = 1.43 \times 10^{22}$ cm^{-3} is the concentration of the Mn sites in LSMO. The values of $g(\mu)$ evaluated with equation (11) are collected in table 2. The values of α for the Mott VRH conductivity regimes, displayed in table 2, are obtained using the first of equations (3) under the assumption of universality of $g(\mu)$ in various temperature intervals. It can be seen that the influence of Fe doping y on the localization radius results in a weak increase of α, whereas the values of α in different temperature intervals are close to each other, excluding the interval LTM in #20. However, α does not exceed the maximum radius for small lattice polarons, $r_p^{max} = 2(4\pi N_s/3)^{-1/3} \approx 5.4$, 5.5 and 5.6 Å for #15, 20 and 25, respectively.

To analyze the SE-like VRH conductivity in #25 one should take into account the existence of the gaps Δ and δ in the DOS spectrum (see section 1). The value of $\Delta \approx 0.30$ eV can be found with the second of equation (5), where $T_{VSE} \approx 150$ K (section 4.2) and T_{SE} is taken from table 1. The value of $\kappa \approx 3.6$ is found with the relation $\Delta \approx U$, where $U \approx e^2/(\kappa R)$ is the mean energy of the Coulomb interactions and $R \approx 2[4\pi N_0(c_0 - y)/3]^{-1/3}$ is the mean distance between the charge carriers or Mn^{4+} involved in the hopping. Then $\delta_V \approx 0.07$ eV is evaluated with the first of equations (5), whereas α in the interval SE of #25 Å (table 2) is found with the second of equations (3). As can be seen in table 2, the value of α in the SE interval of #25 above T_C is enhanced with respect to those in #15 and #20 at $T > T_C$. Such enhancement is attributable to proximity to the metal–insulator transition, induced by doping with Fe (y-MIT). Indeed, the SE interval of #25 can be regarded as the result of evolution of the interval of the metallic behavior of $\rho(T)$ in #15 via the interval between two inflections of $\rho(T)$ in #20 (those intervals are defined as ΔT in section 2). Then, a critical behavior of $\alpha = \alpha^*(1 - c/c_{cr})^{-\nu}$, similar to the behavior near the Anderson transition [16], is expected inside the interval ΔT. Here $c_{cr} \approx c_0 - y_{cr}$, where y_{cr} corresponds to y-MIT, $\nu \approx 1$ and α^* is the value of α far from y-MIT, given by the universal Mott criterion, $N_{cr}^{1/3}\alpha^* \approx 0.25$ [16], where $N_{cr} = N_0(1 - y_{cr})$. This yields the expression $\alpha(y) \approx 0.25[N_0(1 - y_{cr})]^{-1/3} [(c_0 - y_{cr})/(y - y_{cr})]$. Substituting into this equation the

values of $y = 0.25$ and $\alpha(y) = \alpha(\text{SE})$ from table 2, one finds $y_{\text{cr}} \approx 0.18$, between those of #15 ($y = 0.15$) and #20 ($y = 0.20$). This means proximity of #15 to y-MIT from the metallic side and closeness of #20 to y-MIT from the insulating side. This is in complete agreement with the metallic behavior of $\rho(T)$ in #15 and activated behavior, accompanied by two inflections, of $\rho(T)$ in #20 in the interval ΔT. The value of $\alpha^* \approx 0.25[(1 - y_{\text{cr}})N_0]^{-1/3} \approx 1.1$ Å is close to $\alpha = 1.0$–1.2 in table 2 in the temperature intervals HTM and ITM outside ΔT (but above or near T_{C}) where the y-MIT does not take place.

4.5. Final remarks to the discussion

Preliminarily, one should mention the close values of W in LSMFO and in LSMO, as found from analysis of the magnetic properties in section 4.1. Hence, unlike LCMFO [21], the decrease of T_{C} with y in LSMFO can be explained by damping of DE interactions alone, whereas the influence of an additional disorder induced by doping with Fe is not observed. At this point it is important to recall the value of $q = 0$, characteristic of all our investigated LSMFO samples, as obtained in section 4.2, implying absence of the fluctuating short-range potential in LSMFO up to $y = 0.25$ (section 3). The latter is in line with the absence of the influence of disorder, induced by doping with Fe, on the decay of T_{C} with y. On the other hand, such behavior differs considerably from that of LCMFO, where the contribution of the short-range potential to the microscopic disorder (given by $q = 4$, see section 3) already commences from $y = 0.03$ [15]. Therefore, despite the large increase of the resistivity with Fe doping in LCMFO [15] and LSMFO (present work), the role of Fe in LSMFO is limited only to damping of the DE interactions in the Fe^{3+}–Mn^{4+} pairs, whereas the disorder induced by doping with Fe is much less significant.

As discussed at the end of section 4.4, α is sensitive to the electronic phase of LSMFO (proximity to y-MIT), which could explain the enhanced value of α (SE) in #25 above T_{C} (table 2). A sensitivity of α to the magnetic phase of LSMFO is expected, as well. However, a substantial enhancement of α in the FM phase takes place only in #20, but not in #25, where the values of α at $T > T_{\text{C}}$ and at $T < T_{\text{C}}$ (HTM and LTM values in table 2, respectively) are close to each other. On the other hand, such differences of the behavior of α above correlate reasonably with the well-defined FM transition and pronounced FM properties of #20 below T_{C}, whereas the FM transition in #25 is broadened considerably and its FM properties are weakened (cf the bottom panel of figure 1).

Concerning the magnetic field dependence of the microscopic parameters, α and $g(\mu)$, one should pay attention to the following features. First of all, the decrease of DOS in the magnetic field is expected, due to the corresponding increase of the effective electron bandwidth (cf equation (11)). This bandwidth increases as the angle between the spins in the Mn^{3+}–Mn^{4+} pairs [8–10] is decreased by their alignment in the applied magnetic field. The increase of W with B stimulates an increase of $\alpha(B)$ as well, making the hopping of electrons between $Mn^{3+,4+}$ sites easier when the localized magnetic

moments of the neighboring ions are aligned better [8–10]. Therefore, different $\alpha(B)$ and $g(B)$ dependences in various temperature intervals (figure 5) indicate the existence of phases characterized by the different sensitivity of the Mn ion spins to the magnetic field.

The weakening of the dependences of $\alpha(B)$ and $g(B)$ between #15 and #20 in the interval HTM (figure 5) is in line with the breaking of the DE interactions by doping with Fe. At this point, one should mention the violation of the quadratic field dependence of $\alpha(B)$, characteristic of the PM phase (see [33] and equation (7)), in the interval HTM in as low a field as $B = 2$ T. The latter means that the interval HTM, characterized by the relation of $T > T_{\text{C}}$ at $B = 0$, exhibits features of the PM phase only partially, when exposed to a sufficiently low magnetic field. On the other hand, the width of the FM transition is already broadened appreciably at $B = 100$ mT, which is attributable to the increase of the fraction of the second, hole-rich FM phase with increasing B (cf the bottom panel of figure 2 and the corresponding discussion in section 4.1). This explains the violation of the behavior of $\alpha(B)$, given by equation (7), in the interval HTM for $B > 2$ T, presented in such fields by a mixture of the PM and FM phases, due to the phase separation effect [6].

Comparing with other manganites, the value of $\Delta \approx 0.3$ eV in #25 is smaller than $\Delta \approx 0.4$–0.5 eV in LCMFO [15], LBMO [26] and LMO [27, 28]. This is connected to the smaller concentration of the holes or Mn^{4+}, involved in the hopping, $c \approx 0.061$ in #25 against $c \approx 0.20$–0.30 [15, 26–28] in the latter compounds, leading to weaker Coulomb interactions of the charge carriers. This reason is likely to be responsible for observation of only the Mott VRH conductivity in LSMFO at $T > T_{\text{C}}$, whereas in other manganites, mentioned above, the SE VRH conductivity takes place both above [15, 26–28] and below [26] T_{C}. The value of $\kappa \approx 3.6$, obtained in section 4.4, is close to those of $\kappa \approx 3.0$–3.7 [15, 26–28] determined in other manganites from analysis of the hopping conductivity (the reason for the smallness of κ in manganites is discussed in [26]). The value of $\delta_V \approx 0.07$ eV in #25 (section 4.4) is smaller, but quite comparable with the width of the rigid gap, $\delta_V \approx 0.12$–0.28 eV, whereas α in table 2 is typical of the localization radius, $\alpha \approx 1.2$–2.9 Å, of small polarons found in the aforementioned manganite perovskites [15, 26–28], supporting the results of this work.

5. Conclusions

We have investigated the influence of Fe doping on the electronic and magnetic properties of $La_{1-x}Sr_xMn_{1-y}Fe_yO_3$ with $x = 0.3$ and $y = 0.03$ to 0.25, paying major attention to the behavior of $\rho(T)$ and the mechanisms of the hopping conduction in different temperature intervals between 310 and 5 K in magnetic fields up to 8 T. A strong decrease of the ferromagnetic Curie temperature with y is observed, which is determined by breaking of the double-exchange interactions in the Fe^{3+}–Mn^{4+} pairs. A strong overall increase of the resistivity with increasing y of LSMFO takes place, accompanied by transformation of the metallic conduction at $y = 0.03$ into the activated conductivity at $y = 0.25$

within the whole range of investigated temperatures. The Mott and the Shklovskii–Efros variable-range hopping conductivity mechanisms have been identified and analyzed in LSMFO samples with different y in various temperature intervals. The zero-field values of the microscopic parameters, such as the localization radius α, the density of the localized states near the Fermi level $g(\mu)$ and the widths of the soft Coulomb and of the rigid gaps have been determined, and the dependence of α and $g(\mu)$ on the magnetic field have been obtained and discussed.

References

[1] Moritomo Y, Asamitsu A and Tokura Y 1997 *Phys. Rev.* B **56** 12190
[2] Tiwari A and Rajeev K P 1999 *J. Appl. Phys.* **86** 5175
[3] Huang Q, Li Z W and Ong C K 2001 *J. Appl. Phys.* **89** 7410
[4] Chashka K B, Fisher B, Genossar J, Patlagan L and Reisner G M 2001 *Phys. Rev.* B **63** 064403
[5] Yanchevsjii O Z, V'yunov O I and Belous A G 2006 *Low Temp. Phys.* **32** 134
[6] Pashchenko V P, Shemyakov A A, Pashchenko A V, Prokopenko V K, Revenko Yu F, Turchenko V A and Varyukhin V N 2007 *Low Temp. Phys.* **33** 663
[7] Von Helmolt R, Wecker J, Holzapfel B, Schulz L and Sammer K 1993 *Phys. Rev. Lett.* **71** 2331
Schiffer P, Ramirez A P, Bao W and Cheong S-W 1995 *Phys. Rev. Lett.* **75** 3336
[8] Ramirez A P 1997 *J. Phys.: Condens. Matter* **9** 8171
[9] Coey J M D, Viret M and von Molnar S 1999 *Adv. Phys.* **48** 167
[10] Tokura Y (ed) 2000 *Colossal Magnetoresistive Oxides* (Amsterdam: Gordon and Breach)
[11] Dagotto E 2002 *Nanoscale Phase Separation and Colossal Magnetoresistance* (Berlin: Springer)
[12] Wollan E O and Koehler W C 1955 *Phys. Rev.* **100** 545
[13] Töpfer J and Goodenough J B 1997 *J. Solid State Chem.* **130** 117
[14] Worledge D C, Snyder G J, Beasley M R and Geballe T H 1996 *J. Appl. Phys.* **80** 5158
[15] Laiho R, Lisunov K G, Lähderanta E, Petrenko P A, Salminen J, Shakhov M A, Safontchik M O, Stamov V S, Shubnikov M V and Zakhvalinskii V S 2002 *J. Phys.: Condens. Matter* **14** 8043
[16] Mott N F and Davies E A 1979 *Electron Processes in Non-Crystalline Materials* (Oxford: Clarendon)
Mott N F 1990 *Metal–Insulator Transitions* (London: Taylor and Francis)
[17] Shklovskii B I and Efros A L 1984 *Electronic Properties of Doped Semiconductors* (Berlin: Springer)
[18] Ahn K H, Wu X W, Liu K and Chien C L 1996 *Phys. Rev.* B **54** 15299
[19] Jonker G H 1954 *Physica* **20** 1118
[20] Ahn K H, Wu X W, Liu K and Chien C L 1997 *J. Appl. Phys.* **81** 5505
[21] Laiho R, Lisunov K G, Lähderanta E, Salminen J and Zakhvalinskii V S 2002 *J. Magn. Magn. Mater.* **250** 267
[22] Viret M, Ranno L and Coey J M D 1997 *Phys. Rev.* B **55** 8067
[23] Hasanain S K, Nadeem M, Shah W H, Akhtar M J and Hasan M M 2000 *J. Phys.: Condens. Matter* **12** 9007
[24] Sun Y, Xu X and Zhang Y 2000 *J. Phys.: Condens. Matter* **12** 10475
[25] Biswas A, Elizabeth S, Raychaudhuri A K and Bhat H L 1999 *Phys. Rev.* B **59** 5368
[26] Laiho R, Lisunov K G, Lähderanta E, Shakhov M A, Stamov V N, Zakhvalinskii V S, Kozhevnikov V L, Leonidov I A, Mitberg E B and Patrakeev M V 2005 *J. Phys.: Condens. Matter* **17** 3429
[27] Laiho R, Lisunov K G, Lähderanta E, Stamov V N, Zakhvalinskii V S, Colomban Ph, Petrenko P A and Stepanov Yu P 2005 *J. Phys.: Condens. Matter* **17** 105
[28] Laiho R, Lisunov K G, Lähderanta E, Shubnikov M L, Stepanov Yu P, Petrenko P A, Khokhulin A and Zakhvalinskii V S 2006 *J. Phys.: Condens. Matter* **18** 10291
[29] Laiho R, Lisunov K G, Lähderanta E, Petrenko P, Stamov V N and Zakhvalinskii V S 2000 *J. Magn. Magn. Mater.* **213** 271
[30] Laiho R, Lisunov K G, Lähderanta E, Zakhvalinskii V S, Kozhevnikov V L, Leonidov I A, Mitberg E B and Patrakeev M V 2005 *J. Magn. Magn. Mater.* **293** 892
[31] Laiho R, Lisunov K G, Lähderanta E, Petrenko P, Salminen J, Stamov V N, Stepanov Yu P and Zakhvalinskii V S 2003 *J. Phys. Chem. Solids* **64** 2313
[32] Matveev V N, Ylinen E, Zakhvalinskii V S and Laiho R 2007 *J. Phys.: Condens. Matter* **19** 226209
[33] Varma C M 1996 *Phys. Rev.* B **54** 7328